Detection of slow-moving targets in sea clutter by HRR generalized detector

Vyacheslav Tuzlukov*
EE School, College of IT Engineering, Kyungpook National University,
1370 Sankyuk-dong, Buk-gu, Daegu 702-701, South Korea

ABSTRACT

The radar detection of targets in the presence of sea clutter has relied upon the radial velocity of targets with respect to the radar platform either by exploiting the relative target Doppler frequency (for targets with sufficient radial velocity) or by discerning the paths targets traverse from scan to scan. For targets with little to no rapid velocity component, though, it can become quite difficult to differentiate targets from the surrounding sea clutter. The present paper addresses the detection of slow-moving targets in sea clutter using the high resolution radar (HRR) based on the generalized detector (GD) constructed in accordance with the generalized approach to signal processing (GASP) in noise such that the target has perceptible extent in range. Under the assumption of completely random sea clutter spikes based on a ε-contaminated mixture model with the signal and clutter powers known, the best detection performance results from using the GD and is compared with that of the likelihood ratio test (LRT GD). For realistic sea clutter, the clutter spikes tend to be a localized phenomenon. Based upon observations from real radar data measurements, a heuristic approach exploiting a salient aspect of the idealized GD is developed which is shown to perform well and possesses superiority over the LRT GD performance when applied to real measure sea clutter.

Keywords: Generalized detector, synthetic aperture radar, high resolution radar, likelihood ratio test, likelihood ratio function, noncoherent detection, Neyman-Pearson criterion.

1. INTRODUCTION

High resolution radar (HRR) is able to resolve individual scattering centers over the radial range extent of target relative to the range resolution capability of the radar[1]. The radar range resolution is typically inversely proportional to the transmitted radar waveform bandwidth. Wideband (WD) and ultra wideband (UWD) radars operate at bandwidth of hundreds of MHz to a few GHz and obtain range resolutions on the order of a meter down to a few centimeters. Radar systems employing such high bandwidths, for example, synthetic aperture radar (SAR) and inverse SAR (ISAR) are often used for imaging purposes such as mapping and target identification/discrimination[2]. Besides imaging, the HRR may provide a means of achieving substantial improvement in target detection performance compared with lower range resolution radar, for example, a typical pulse-Doppler radar with resolution on the order of tens meters. The potential detection improvement arises because HRR range cells are small enough such that reflected return signals from different scattering centers (from targets or clutter) can be individually resolved. In contrast, lower resolution radars, such as pulse-Doppler, receive a superposition of return signals from clutter and possibly targets in each range cell thus requiring clutter cancellation in order to extract the targets. In the case of land clutter, the clutter returns are pervasive thus relegating HRR to require clutter cancellation or rely on target motion in order to adequately detect targets. However, at low grazing angles, sea clutter is found to be relatively sparse[3–8], i.e. only a relatively small number of range cells contain significant sea clutter returns. Hence, targets in sea clutter may be observed through the clutter and potentially detected by discriminating the target from the clutter signature. In general, such an approach can be referred to as an "image-to-detect" method where some innate characteristic of a target can be used to differentiate it from the clutter. Specifically, track-before-detect approaches[9–11] have been proposed to differentiate targets from clutter which search for paths traversed by moving targets over several scans. Such approaches typically employ some version of the Hough transform[12] to extract the location and bearing of straight line paths or perhaps even simple curved paths[13] within the limits of the image comprised of the range-gated return signals from a set of consecutive scans illuminating the same spatial region. However, as with pulse-Doppler radar, track-before-detect approaches require some radial target motion with respect to the radar platform

*tuzlukov@ee.knu.ac.kr; phone +82 053 950-5509; fax +82 052 950-5505; spl.ee.knu.ac.kr

Signal Processing, Sensor Fusion, and Target Recognition XXI, edited by Ivan Kadar,
Proc. of SPIE Vol. 8392, 83921L · © 2012 SPIE · CCC code: 0277-786X/12/$18 · doi: 10.1117/12.919844

and therefore may not work well for targets that have little or no radial motion over a given processing window. Conceptually, an image-to-detect methodology could exploit any available knowledge of the targets and/or clutter in order to discriminate between the two. As such, in addition to being sparse in nature, sea clutter observed from low grazing angles can also be characterized as being highly localized, i.e. clusters of sea clutter associated with wave crests [14], and spiky [7,8] when present, returns can be quite large and often called sea spikes or clutter spikes, as well as nonstationary [3] due to the motion of the sea surface. Numerous statistical models such as Weibull, log-normal, *K*, compound-Gaussian, Rayleigh, and Ricean [15–22] have been employed to characterize sea clutter and subsequently develop corresponding detectors [23–26] though typically for moving targets with sufficient Doppler. Due to the complex dynamic nature of sea clutter, though, no single type of statistical model is always applicable [27]. Instead, we focus on simple quantities of the sea clutter, such as the average range extent and temporal persistence of localized clusters of sea spikes which can be readily measured for given geographical regions and sea states. This information can be employed as *a priori* knowledge to implement heuristic detectors capable of discriminating slow-moving or stationary targets from the sea clutter. This paper addresses the detection of slow-moving or stationary targets in sea clutter using the generalized detector (GD) constructed in accordance with the generalized approach to signal processing in noise [28–33] and employed by HRR. Initially, we use a simple ε-contaminated Gaussian model as a first-order approximation of sea clutter at low grazing angles to represent the sparse nature of the sea clutter spikes and, assuming the clutter and target powers are known, formulate a likelihood ratio test for GD (LRT GD). For the scenario represented by the ε-contaminated Gaussian model, the LRT GD is the optimal under the Neyman-Pearson criterion and is compared with the conventional LRT. However, as expected the LRT GD is found to perform poorly in the presence of real sea clutter because the ε-contaminated Gaussian model does not incorporate the localization aspect in range and time (pulse space) such it occurs for real sea clutter. As will be shown, the likelihood ratio function (LRF) suggests the use of a limiter on the received data as a means of robustness against high clutter power relative to the target power. Accounting for the localized nature of the sea clutter spikes, this then leads to the development of the noncoherent slow target GD (NST GD) algorithm. Succinctly, NST GD is comprised of an initial binary GD on each individual range cell for a set of consecutive pulses within a single scan followed by a sliding window averaging filter across range to extract targets with sufficient range extent and then integration of each range cell over the set of pulses in the scan to ensure target persistence and reduce false alarms. For both randomly generated ε-contaminated Gaussian data and real measured sea clutter data, detection performance curves are obtained for the LRT GD and NST GD and compared with the conventional GLRT. It will be shown that for the ε-contaminated Gaussian data that NST GD closely approaches the optimal GD performance established by LRT GD while for real sea clutter data NST GD is far superior to the LRT GD.

2. DETECTION USING SPARSE CLUTTER MODEL

2.1 Basic GD functioning principles

For better understanding, we recall the main functioning principles of GD. The simple model of GD in form of block diagram is represented in Fig.1. In this model, we use the following notations: MSG is the model signal generator (local oscillator), the *AF* is the additional filter (the linear system) and the *PF* is the preliminary filter (the linear system). A detailed discussion of the *AF* and *PF* can be found in [28,30] .Consider briefly the main statements regarding the *AF* and *PF*. There are two linear systems at the GD front end that can be presented, for example, as bandpass filters, namely, the *PF* with the impulse response $h_{PF}(\tau)$ and the *AF* with the impulse response $h_{AF}(\tau)$. For simplicity of analysis, we think that these filters have the same amplitude-frequency responses and bandwidths. Moreover, a resonant frequency of the *AF* is detuned relative to a resonant frequency of *PF* on such a value that signal cannot pass through the *AF* (on a value that is higher the signal bandwidth). Thus, the signal and noise can be appeared at the *PF* output and *the only noise* is appeared at the *AF* output. It is well known, if a value of detuning between the *AF* and *PF* resonant frequencies is more than $4 \div 5\Delta f_a$, where Δf_a is the signal bandwidth, the processes forming at the *AF* and *PF* outputs can be considered as independent and uncorrelated processes. In practice, the coefficient of correlation is not more than 0.05. In the case of "no" signal in the input process, the statistical parameters at the *AF* and *PF* outputs will be the same, because the same noise is coming in at the *AF* and *PF* inputs, and we may think that the *AF* and *PF* do not change the statistical parameters of input process, since they are the linear GD front end systems. By this reason, the *AF* can be considered as a reference sample source with *a priori* information *a "no" signal is obtained in the additional reference noise* forming at the *AF* output. There is a need to make some comments regarding the noise forming at the *PF* and *AF* outputs. If the Gaussian noise $w(t)$ comes in at the *AF* and *PF* inputs (the GD linear system front end), the noise formed at the *AF* and *PF* outputs is

Gaussian, too, because the AF and PF are the linear systems and, in a general case, take the following form:

$$n_{PF}(t) = \xi(t) = \int_{-\infty}^{\infty} h_{PF}(\tau) w_l(t-\tau_l) d\tau \quad \text{and} \quad n_{AF}(t) = \eta(t) = \int_{-\infty}^{\infty} h_{AF}(\tau) w_l(t-\tau_l) d\tau \quad . \tag{1}$$

If the additive white Gaussian noise (AWGN) with zero mean and two-sided power spectral density $0.5N_0$ is coming in at the AF and PF inputs (the GD linear system front end), then the noise forming at the AF and PF outputs is Gaussian with zero mean and variance given by [30] $\sigma_n^2 = \frac{N_0 \omega_0^2}{8\Delta_F}$, where in the case if AF (or PF) is the RLC oscillatory circuit, the AF (or PF) bandwidth Δ_F and resonance frequency ω_0 are defined in the following manner $\Delta_F = \pi\beta, \omega_0 = \frac{1}{\sqrt{LC}}, \beta = \frac{R}{2L}$.

The main functioning condition of GD is an equality over the whole range of parameters between the model signal forming at the GD MSG output for user l and the expected signal forming at the GD input liner system (the PF) output. How we can satisfy this condition in practice is discussed in detail in [28,30]. More detailed discussion about a choice of PF and AF and their amplitude-frequency responses is given in [31] (see http://www.sciencedirect.com/science/journal/10512004, click "Volume 8, 1998", "Volume 8, Issue 3", and "A new approach to signal detection theory").

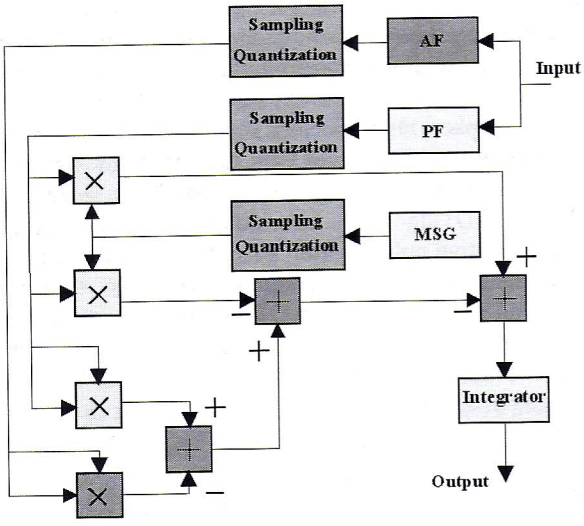

Figure 1. Principal flowchart of GD.

2.2 Sparse clutter model

For high radar range resolution, sea clutter spikes are sparse and may have a relatively high clutter-to-noise ratio (CNR). To gain some insight into the appropriate form that a detector must take in order to contend with sparse, spiky clutter with high CNR, we use a first-order approximate model for the clutter discussed in [34] (probabilistically in terms of the clutter spike rate of occurrence) based upon ε-contaminated Gaussian model [15,16]. The ε-contaminated Gaussian model is applicable because it aptly represents the sparseness of the clutter whereby ε is the fraction of range cells over all pulses containing both clutter spikes and noise and $1-\varepsilon$ is the fraction containing only noise. It will be shown that features of the GD resulting from this model suggest a particular form for the detection of range-distributed targets in real sea clutter For P consecutive pulses illuminating a spatial region within a single scan and B range cells between the minimum range $R_{\min}$ and maximum range $R_{\max}$, the parameter ε is the percentage of the total PB range cells which contain sea clutter. GD is to be applied to a set of K samples of the return data with the $K = P\hat{B}$ samples being a block of data taken from $\hat{B}$ contiguous range cells across all P pulses. GD is applied to the K data samples formed from each set of $\hat{B}$ contiguous range cells among the total B range cells. Under the standard binary hypothesis test according to the generalized approach to signal processing in noise,

$$x_k = \eta_k \rightarrow H_0; \qquad k = 1, \ldots, K \tag{2}$$

is the interference only case, where η_k is comprised of noise and clutter according to the ε-contaminated Gaussian model;

$$x_k = s_k + \xi_k \rightarrow H_1 ; \qquad k = 1, \ldots, K \tag{3}$$

is the target-plus-interference case, where s_k is the target return signal (Subsection 2.1). It is assumed that the K samples are independent and identically distributed (i.i.d.) and the received signal powers are normalized by the internal noise such that, without loss of generality, the noise power is set to unity. For complex Gaussian internal noise and assuming the sea clutter spikes are also complex Gaussian with the variance (power) σ_c^2, the probability density function (pdf) of $y_k \equiv | x_k |^2$ for a given range cell using the ε-contaminated Gaussian model under the hypothesis H_0 is

$$f_{H_0}(y_k) = \frac{\varepsilon}{\sigma_c^2 + 1} \exp\left\{-\frac{y_k}{\sigma_c^2 + 1}\right\} + (1-\varepsilon)\exp\{-y_k\} \ . \tag{4}$$

Similarly, assuming the target return signal for a given range cell is the complex Gaussian with the variance (power) σ_s^2, the pdf under hypothesis H_0 takes the following form

$$f_{H_1}(y_k) = \frac{\varepsilon}{\sigma_s^2 + \sigma_c^2 + 1} \exp\left\{-\frac{y_k}{\sigma_s^2 + \sigma_c^2 + 1}\right\} + \frac{1-\varepsilon}{\sigma_s^2 + 1} \exp\left\{-\frac{y_k}{\sigma_s^2 + 1}\right\} \ . \tag{5}$$

If σ_s^2 and σ_c^2 are known, the LRT GD is optimal and takes the form

$$L(y) = \frac{\prod_{k=1}^{K} f_{H_1}(y_k)}{\prod_{k=1}^{K} f_{H_0}(y_k)} \underset{H_0}{\overset{H_1}{\gtrless}} K_{GD} \ , \tag{6}$$

where $L(y)$ is the LRF and K_{GD} is the GD threshold. We assume that the clutter power σ_c^2 can be fairly accurately estimated, the amount of clutter contamination ε may only be known to within some range of values $\Omega_\varepsilon = [\varepsilon_{\min}, \varepsilon_{\max}]$. In addition, the target return signal power σ_s^2 cannot be known *a priori* but may be bounded to lie within $\Omega_s = [\sigma_{s\,\min}^2, \sigma_{s\,\max}^2]$ where $\sigma_{s\,\min}^2$ is some nominally detectable target power and $\sigma_{s\,\max}^2$ is the largest expected target power. Assuming that ε and σ_s^2 are independent and uniformly distributed over Ω_ε and Ω_s, respectively, such that

$$f_{H_0}(y, \varepsilon) = f_{H_0}(y \mid \varepsilon) f(\varepsilon) \ ; \tag{7}$$

$$f_{H_1}(y, \varepsilon, \sigma_s^2) = f_{H_1}(y \mid \varepsilon, \sigma_s^2) f(\varepsilon) f(\sigma_s^2) \ . \tag{8}$$

Integrating ε and σ_s^2 out of the joint pdfs (7) and (8), the optimal log-LRF after minor simplification takes the form:

$$\ln L(y) = \sum_{k=1}^{K} \left\{ \ln \int_{\Omega_\varepsilon, \Omega_s} f_{H_1}(y_k \mid \varepsilon, \sigma_s^2) d\varepsilon \, d\sigma_s^2 - \ln \int_{\Omega_\varepsilon} f_{H_0}(y_k \mid \varepsilon) d\varepsilon + C \right\} \ , \tag{9}$$

where C is a constant. Hence, setting

$$f(y_k) = \ln \int_{\Omega_\varepsilon, \Omega_s} f_{H_1}(y_k \mid \varepsilon, \sigma_s^2) d\varepsilon \, d\sigma_s^2 - \ln \int_{\Omega_\varepsilon} f_{H_0}(y_k \mid \varepsilon) d\varepsilon \tag{10}$$

yields the LRT GD with the form

$$\sum_{k=1}^{K} f(y_k) \underset{H_0}{\overset{H_1}{\gtrless}} K_{GD} \ . \tag{11}$$

Note that the LRT GD algorithm in (11) is not optimal for any particular value of σ_s^2 in Ω_s or ε in Ω_ε but is optimal over all the values of Ω_ε and Ω_s in aggregate. For realistic combinations of parameters ε and σ_s^2 the log-LRT GD component function $f(y_k)$ has a step-like response. The step-like nature of the log-LRT GD component function $f(y_k)$ essentially acts as a limiter which removes the effects of high clutter power and thereby enables the GD to rely instead of the density of sufficiently large target return signals over the K samples. This like-step nature of the log-LRT GD component function $f(y_k)$ for idealized random clutter is used as the basis for the heuristic NST GD that is considerably more robust than the LRF for real sea clutter which tends to be highly localized.

3. NST GD ALGORITHM

3.1 NST GD designing principles

The step-like nature of the LRF provides an insight into dealing with sparse clutter in which the clutter spikes may have much higher power than any target return signal present. For input powers above some value, the LFR is quite similar to a limiter or clipping function. Any dominance of high power clutter spikes over the lower power targets is therefore removed since any target return signals that have power levels that fall within the limits of the clipped region of the LFR yield essentially the same output. Hence, it is not so much the power levels that determine detectability as it is the rate of incidence of sufficiently high target return signals within the set of samples under test. While the limiter aspect of the LFR removes the clutter power dominance, the real sea clutter is found to be much more localized in range and time (pulse space) than the ε-contaminated Gaussian model based on (5) and (6) which is randomly distributed. As a result, the combination of the LRF outputs from K samples via simple simulation as in (12) can lead to a very high false alarm rate for real sea clutter. To compensate, we replace the summation with two successive M-of-N GD as it is discussed in [35] to ensure that the target return signals cover a sufficient range extent and persist for long enough to be declared a target. Given *a priori* knowledge via measurement of the sea clutter and current sea state, the number of clutter false alarms can be greatly reduced. Therefore, for targets with sufficient range extent and temporal persistence the probability of detection can be substantially enhanced over the LRT when in real sea clutter. For the P pulses within the limits of the same scan and L range cell target return signals from each pulse, the power associated with the l -th range cell of the p-th pulse is denoted as $y_{p,l}$ for $l = 0,\ldots,L-1$ and $p = 0,\ldots,P-1$. The NST GD approach is comprised of three stages. The first stage is a binary GD that is essentially a simplified version of the LRF GD in which the threshold K_{GD} is set according to the quiescent noise level, i.e., the clutter free. Values of $y_{p,l}$ with magnitudes surpassing the binary GD threshold as

$$\left[y_{p,l} \gtrless K_{GD}\right] \rightarrow d_{p,l}^{(1)} \tag{12}$$

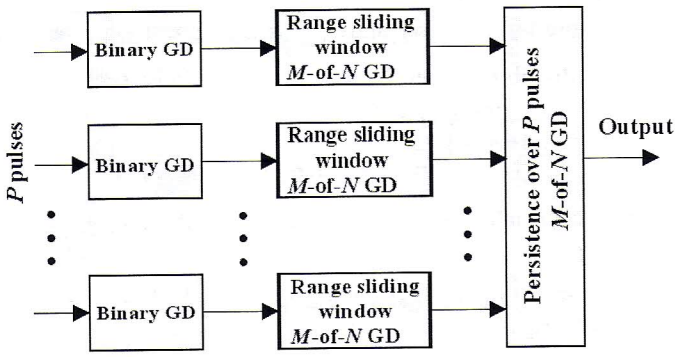

Figure 2. NST GD algorithm.

are set to 1 while others are set to 0 with the output of the binary GD for the l -th range cell of the p-th pulse being denoted as $d_{p,l}^{(1)}$. As a result, an influence of large range cell powers is removed from later detection strategies thereby mitigating possible dominance by high clutter powers. The second stage of NST GD operates upon the L binary-detected range target return signals for each of the individual P pulses to determine if some local range region has a high density of detectable target return signals thereby indicating the probable presence of a target. This is done by employing a sliding window version of M-of-N GD for which the parameters are denoted as M_2 and N_2. The sliding window M-of-N GD is such that for each range-shift index $l_r \in [0,\ldots,L-N_2+1]$ for the p-th pulse, the GD output $d_{p,l}^{(2)}$ is set to either 0 or 1 according to

$$\left\{ \sum_{l=l_r}^{l_r+N_2-1} d_{p,l}^{(1)} \gtrless M_2 \right\} \rightarrow d_{p,l}^{(2)} \quad . \tag{13}$$

The values of N_2 and M_2 can be determined according to a histogram of sea spike range extents for a given sea state at a given location. The third and final stage of NST GD operates on the range GD output $d_{p,l}^{(2)}$ across the P pulses for each range-shift index l_r to determine persistence. This is accomplished by applying another M-of-N GD with parameters $N_3 = P$ and M_3 as

$$\left\{ \sum_{p=0}^{P-1} d_{p,l}^{(2)} \underset{<}{\geq} M_3 \right\} \rightarrow d_{p,l}^{(3)} \quad . \tag{14}$$

Figure 2 illustrates the overall operation of the proposed NST GD algorithm. The first stage of the NST GD algorithm is a simplification of the LRF which essentially serves the purpose to remove the power dominance of the clutter spikes. However, while the LRT GD is performed on the sum of the clipped outputs for all of the pulse/range input samples, NST GD algorithms applies separate GDs in range and over the pulses. In so doing, NST GD algorithm can be made to be considerably more robust than the LRT GD by appropriately adjusting the separate GD thresholds.

3.2 NST GD false alarm definition

Because the NST GD algorithm employs a simplified version of the LRF that takes the form of discrete GD, a closed-form solution to the probability of false alarm P_{FA} can be found for NST GD under the ε-contaminated Gaussian model. From the perspective of a single range/pulse sample that is input to the discrete GD at the first stage of NST GD, the probability of false alarm P_{FA} on a given individual discrete GD, which we denote as P_{FA_1} can be expressed as

$$P_{FA_1} = \varepsilon \exp\left\{ -\frac{K_{GD}}{4\sigma_c^4 + 1} \right\} + (1-\varepsilon)\exp\{-K_{GD}\} \quad , \tag{15}$$

where it is assumed that the input signal has been normalized such that the noise power is unity. The false alarm probabilities for the second and third stages can then be readily found by summing over the false alarm occurrences of the binomial pdf as

$$P_{FA_2} = \sum_{m=M_2}^{N_2} \binom{N_2}{m} P_{FA_1}^m (1-P_{FA_1})^{N_2-m} \tag{16}$$

and

$$P_{FA} = P_{FA_3} = \sum_{m=M_3}^{N_3} \binom{N_3}{m} P_{FA_2}^m (1-P_{FA_2})^{N_3-m} \tag{17}$$

with (17) being the overall false alarm probability for NST GD given the ε-contaminated signal model for the clutter.

3.3 NST GD parameter selection

The proper selection of the NST GD operating parameters K_{GD}, N_2, M_2, N_3, and M_3 is predicated upon the current sea clutter environment. As is shown experimentally, an employment of higher values of M_2 and M_3 enables the use of a lower initial threshold K_{GD} while maintaining the same false alarm probability P_{FA}. The two sequential M-of-N GDs provide robustness to the particular clutter spike distribution in range and over the set of pulses (be it completely random or highly localized). For completely random sea clutter such as the ε-contaminated Gaussian model, the parameters M_2 and M_3 can be set lower and in so doing provide better detection capability for smaller targets. Conversely, for localized sea clutter, M_2 and M_3 should be set just high enough to exclude the local clutter patches which effectively set the lower limit on detectable target size. The parameters N_2 and N_3 need only be set slightly larger than M_2 and M_3, respectively, so that additional sea spikes are not included thereby increasing the false alarm rate.

4. NST GD PERFORMANCE ANALYSIS

To verify the performance of the NST GD algorithm we apply it and the LRT GD to both simulated data under the ε-contaminated Gaussian model and to real measured data. The LRT GD is optimal for the ε-contaminated Gaussian model scenario but will be shown to suffer severe performance degradation when applied to real data due to the highly localized nature of sea clutter spikes. The measured data is VV polarized sea clutter returns which possesses 30.48 cm range resolution, a pulse-repetition frequency (PRF) of 2 kHz, and an antenna beam width of $2.4°$. Sea clutter spikes were found to

be present in approximately 4%, i.e. $\varepsilon = 0.04$, of the range cells over 8,000 pulses with an average CNR of 25 dB. The NST GD and LRT GD are parameterized for $P_{FA} = 10^{-6}$ with $N_2 = N_3 = 30$ for NST GD and $K = N_2 \times N_3 = 900$ for LRT GD. For simplicity we set $M_2 = M_3$ which we will vary from 1 to 30 to determine the appropriate values for each data set. In addition, we examine targets with range extents of $L = 3.05$ m, $L = 6.1$ m and $L \geq 9.15$ m for each clutter environment to determine the appropriate parameterization for each. For both clutter scenarios the target return signals are modeled as having a Gaussian distribution and are i.i.d. over range and time (pulse space).

4.1 First-order sparse clutter model

The simulated data is approximately modeled after the measured data with ε set to 0.04 and the CNR set to 25 dB. For the fixed probability of false alarm $P_{FA} = 10^{-6}$, the threshold K_{GD} is depicted in Fig. 3 as a function of $M_2 = M_3$. It can be seen that beyond the "knee" at $M_2 = M_3 = 6$, the two *M*-of-*N* GDs enable the threshold K_{GD} to be quite small thereby enabling the good target detection performance. To examine the detection performance for different size targets, the detectable signal power for NST GD to achieve the probability of detection of $P_D = 0.9$ is found for each of the three target sizes – 3.05 m, 6.1 m, and 9.15 m – for the same false alarm rate. The results are shown in Fig. 4 along with the LRT GD

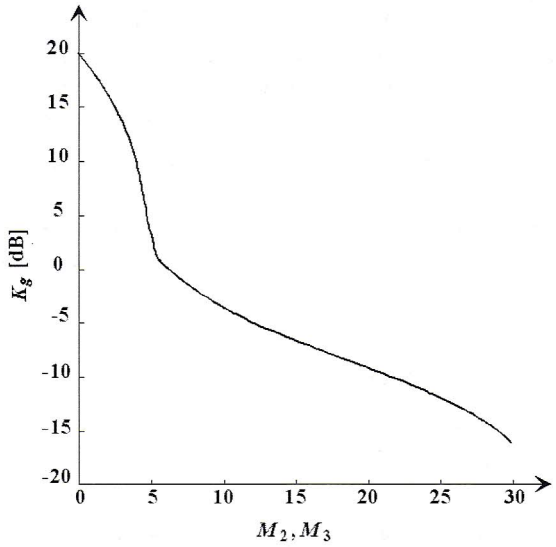

Figure 3. NST GD threshold as a function of M_2, M_3 for the ε-contaminated Gaussian model; $P_D = 0.9$ and $P_{FA} = 10^{-6}$.

target signal powers for $P_D = 0.9$ for each of three targets. As one would be reasonably expect, the target with the greatest extent can be detected with the lowest signal-to-noise ratio (SNR) as there is effectively more target to noncoherent integrate. Furthermore, the $L = 3.05$ m, and $L = 6.1$ m targets are essentially undetectable when using values of M_2 greater than the target extent. For the $L \geq 9.15$ m case the LRT GD is optimal, in aggregate over the values of Ω_ε and Ω_s as discussed previously, and the best performance for NST GD is found when $M_2 = M_3$ are set to 11, 12, or 13, all of which achieve the detectable signal power equal to 0.2dB of optimal. In the case of the $L = 3.05$ m, and $L = 6.1$ m targets the LRT GD is no longer optimal since the targets deviate slightly from the modeled pdf in (6). NST GD reaches the minimal detectable target power at $M_2 = M_3 = 12$ for $L = 6.1$ m which is only 0.05 dB higher than LRT GD and $M_2 = M_3 = 8$ for $L = 3.05$ m which is 0.15 dB lower than LRT GD. Thus, one can conclude that NST GD should be implemented as a bank of GDs parameterized for different sets of similar target sizes. Finally, we examine the detection performance of LRT GD and NST GD for a particular target size of $L = 7.67$ m. The target power is varied for the fixed probability of false alarm $P_{FA} = 10^{-6}$ to generate the detection performance curves for LRT GD and NST GD. The NST GD parameters M_2 and M_3 are both set to 12 with the associated threshold K_{GD} from Fig. 3. Figure 5 shows the resulting detection performance curves where NST GD very closely approaches the optimal bound in aggregate set by the LRT GD. For exam-

ple, for the detectable SNR at the probability of detection of $P_D = 0.9$, NST GD is within approximately 0.13 dB of the LRT GD performance. Comparative analysis with the conventional GLRT detector shows a great superiority of NST and LRT GDs.

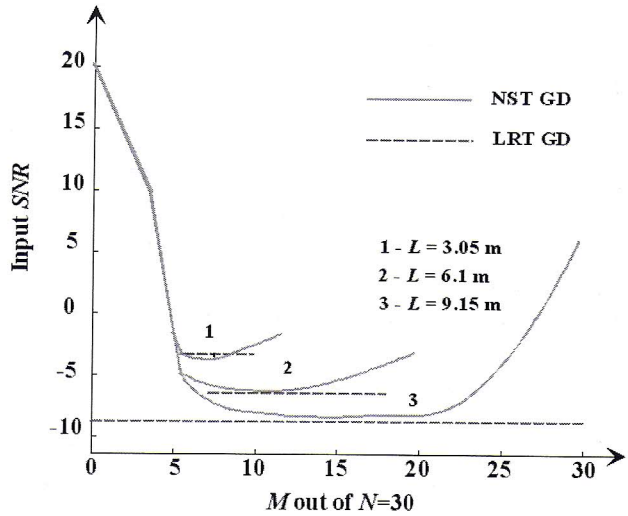

Figure 4. Target signal power for the ε-contaminated Gaussian model; $P_D = 0.9$ and $P_{FA} = 10^{-6}$.

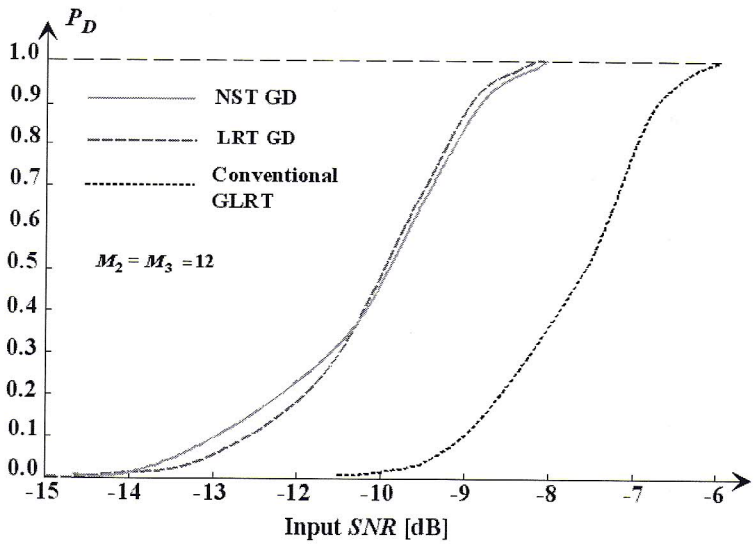

Figure 5. Detection performance of LRT GD and NST GD for the ε-contaminated Gaussian model; $P_{FA} = 10^{-6}$.

4.2 Real measured data

The real measured data is representative of a typical sea clutter "event" in which a significant patch of sea clutters traverses through the region under observation. These "events", which are constituted by large localized areas of clutter spikes, are highly detrimental to the detection of slow/stationary targets because they effectively mask the presence of a target. Due to the finite number of samples of the real measured data, there is a minimum estimate of the false alarm probability that is given by the inverse of the number of data samples. Using the NST GD operating parameters $N_2 = N_3 = 30$ and

for each $M_2 = M_3$ set between 1 and 30, the initial threshold K_{GD} is set at the lowest value such that no false alarms from clutter are detected for any set of 30 contiguous pulses and range cells over all the data resulting in the probability of false alarm of $P_{FA} \leq 10^{-4}$. The threshold K_{GD} which achieves this probability of false alarm P_{FA} is shown in Fig. 6 and is found to decrease much slower as a function of increasing M_2 and M_3 than was the case for the ε-contaminated Gaussian model, note the different values of the probability of false alarm P_{FA}, due to the effects of localized clutter in the measured data. To examine the detection performance for different size targets and M, the M_2 and M_3 for the M-of-N GDs, in real sea clutter, the detectable signal power for NST GD to achieve the probability of detection of $P_D = 0.9$ is found for each of the three target sizes – $L = 3.05$ m, $L = 6.1$ m and $L \geq 9.15$ m – and M for the same probability of false alarm P_{FA}. Figure 7 illustrates the results along with the LRT GD target signal powers for the $P_D = 0.9$ and $P_{FA} \leq 10^{-4}$, note that LRT GD is not a function of M. For the $L = 3.05$ m target, the required input SNR values never reach low levels since the input threshold must be set so high for low values of M_2 and M_3 in order to eliminate the false alarms from the localized sea clutter. Somewhat better performance is achieved for the $L = 6.1$ m target but it is only for the $L \geq 9.15$ m target that a relatively small SNR target can be detected. Compared with NST GD, the performance of the LRT GD for the three target cases is quite poor, with NST GD for $M_2 = M_3 = 28$ needing 18 dB lower SNR than LRT for the $L \geq 9.15$ m target. Note that in contrast to the ε-contaminated Gaussian model no significant minimum is observed. Based on performance for real data it can again be concluded that NST GD should be implemented as detector bank where the individual GDs are appropriately parameterized for different target sizes. For a particular target size of $L = 7.67$ m, the target power is varied for the fixed probability of false alarm $P_{FA} \leq 10^{-4}$ to generate the detection performance curves for LRT GD and NST GD. The NST GD parameters M_2 and M_3 are both set to 24 with the associated threshold K_{GD} from Fig. 6. Figure 8 shows the resulting detection performance curves whereby NST GD dramatically outperforms the LRT GD. For example, at the probability of detection $P_D = 0.9$ NST GD performance is approximately 4.5 dB lower than LRT GD. Comparison with the conventional GLRT detector demonstrates a great superiority under employment of the NST and LRT GDs.

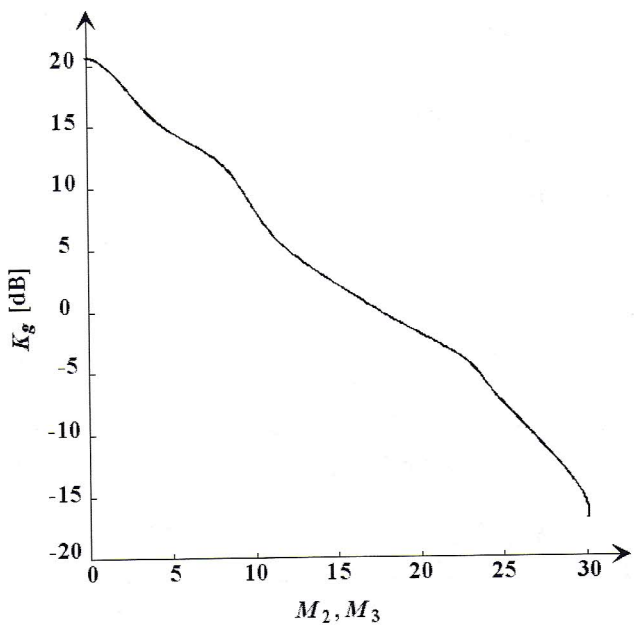

Figure 6. Initial NST GD threshold as a function of M_2, M_3 for real measured data; $P_{FA} = 10^{-4}$.

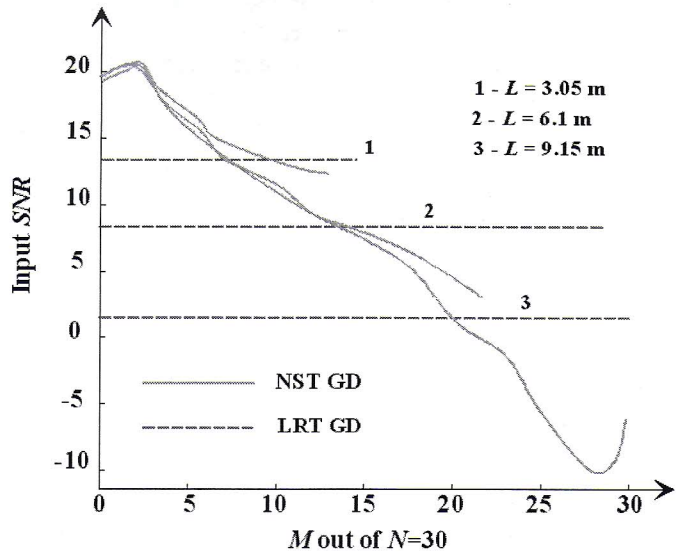

Figure 7. Target signal power for real measured data; $P_D = 0.9$ and $P_{FA} = 10^{-6}$.

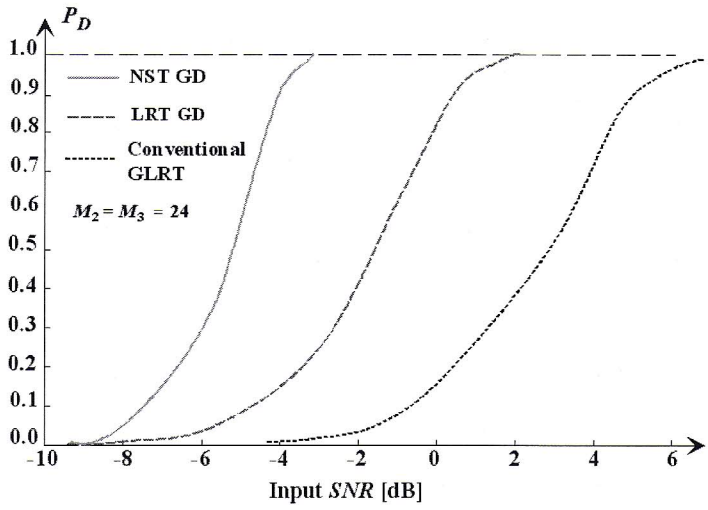

Figure 8. Detection performance of LRT GD and NST GD for the real measured data; $P_{FA} = 10^{-6}$.

5. CONCLUSIONS

Due to the tendency of real sea clutter at low grazing angles to be sparse in nature, the ε-contaminated Gaussian model has been employed as the first-order approximation to mathematically represent the clutter. For the ε-contaminated Gaussian model, the LRT GD is formulated which indicates that an appropriate first detection stage when dealing with sparse clutter of potentially high power is to apply some sort of clipping function to remove the power dominance of the clutter. However, the tendency of sea clutter spikes to be highly localized in range and time, i.e. successive pulses, causes performance degradation for the LRT GD as it was modeled on an idealized clutter model. As such, the NST GD employment has been demonstrated to be a robust surrogate for the LRT GD for the detection of slow/stationary targets in the presence of localized sparse sea clutter for high range resolution radar. The operation of NST GD is partially motivated by the LRT GD in that the first stage of detection employs a power clipping mechanism through the use of a simple discrete GD. To combat the effects of localized sea clutter, NST GD performs successive M-of-N detection procedures across range and over contiguous pulses in order to discriminate the range extent and temporal persistence of targets from sea clu-

tter. It has been shown for the idealized clutter scenario based on the ε-contaminated Gaussian clutter model that NST GD performs nearly identical to the optimal LRT GD. Furthermore, for real measured sea scatter data it has been shown that NST GD is quite robust and performs very well. Areas of future research for NST GD or similar approaches are an individual analysis of clutter range extent and persistence as well as the use of more complex discriminators such as target/clutter shape as realized on a range-pulse repetition interval image and polarization effects.

ACKNOWLEDGMENT

This research was supported by the Kyungpook National University Research Grant, 2011.

REFERENCES

1. Wehner, D.R., *High Resolution Radar*, Boston: Artech House, 1995.
2. Voles, R., " Resolving revolutions: Imaging and mapping by modern radar," *IEE Electronics & Communication Engineering Journal*, 1993, No. 2, pp. 3–12.
3. Skolnik, M.I., *Introduction to Radar Systems*, 3rd Ed. New York: McGraw-Hill, 2001.
   Vol. 19, No.1, pp. 12–16.
4. Macdonald, F.C., "Characteristics of radar sea clutter, Part I – Persistent target-like echoes in sea clutter," *Naval Research Laboratory Report*, 1957, Washington D.C., Report 4902, March, 1957.
   2002, Vol. 19, No.1, pp. 29–43.
5. Lewis, B.L. and Olin, I.D., "Some recent observations of sea spikes," in *Proceedings of IEE Radar Conference*, October 25-28, 1977, pp. 115–119.
6. McLaughlin, D.J., Allan, N., Twarog, E.M., and Trizna, D.B., "High resolution polarimetric radar scattering measurements of low grazing angle sea clutter," *IEEE Journal of Oceanic Engineering*, 1995. Vol. 20, No. 3, pp. 166–178.
7. Posner, F. and Gerlach, K., "Sea spike demographics at high range resolutions and very low grazing angles," in *Proceedings of IEEE National Radar Conference*, May 5-8, Huntsville, Alabama, USA, 2003, pp. 38–45.
8. Posner, F.L., "Spiky sea clutter at high range resolutions and very low grazing angles," *IEEE Transactions on Aerospace and Electronic Systems,* 2002, Vol. 38, No. 1, pp. 58–73.
9. Carlson, B.D., Evans, E.D., and Wilson, S.L., "Search radar detection and track with the Hough transform, Pt I: System concept," *IEEE Transactions on Aerospace and Electronic Systems,* 1994, Vol. 30, No. 1, pp. 102–108.
10. Carlson, B.D., Evans, E.D., and Wilson, S.L., "Search radar detection and track with the Hough transform, Pt II: Detection statistics," *IEEE Transactions on Aerospace and Electronic Systems,* 1994, Vol. 30, No. 1, pp. 109–115.
11. Carlson, B.D., Evans, E.D., and Wilson, S.L., "Search radar detection and track with the Hough transform, Pt III: Detection performance with binary integration," *IEEE Transactions on Aerospace and Electronic Systems,* 1994, Vol. 30, No. 1, pp. 116–125.
12. Duda, R.O. and Hart, P.E., "Use of the Hough transformation to detect lines and curves in pictures," *Commun. Assoc. Comput. Mach,* 1972, Vol. 15, No. 1, pp. 11–15.
13. Olson, C.F., "Constrained Hough transforms for curve detection," *Computer Vision and Image Understanding*, 1999, Vol. 73, No. 3, pp. 329–345.
14. Melief, H.W., Greidanus, H., van Genderen, P., and Hoogeboom, P., "Analysis of sea spikes in radar sea clutter data," *IEEE Transactions on Geosciences and Remote Sensing*, 2006, Vol. 44, No. 4, pp. 985–993.
15. Long, M.W., *Radar Reflectivity of Land and Sea*, 2nd Ed. Dedham, MA: Artech House, 1983.
16. Fay, F.A., Clarke, J., and Peters, R.S., "Weibull distribution applied to sea-clutter," in *Proceedings of IEE Radar Conference*, October 25-28, 1977, pp. 101–103.
17. Trunk, G.V. and George, S.F., "Detection of targets in non-Gaussian sea clutter," *IEEE Transactions on Aerospace and Electronic Systems,* 1970, Vol. 6, No. 6, pp. 620–628.
18. Trunk, G.V., "Radar properties of non-Rayleigh sea clutter," *IEEE Transactions on Aerospace and Electronic Systems,* 1972, Vol. 2, No. 3, pp. 196–204.
19. Rangaswamy, M., Weiner, D.D., and Ozturk, A., "Computer generation of correlated non-Gaussian radar clutter," *IEEE Transactions on Aerospace and Electronic Systems,* 1995, Vol. 31, No. 1, pp. 106–116.
20. Chan, H.C., "Radar sea-clutter at low grazing angles," *IEEE Proceedings F – Radar, Sonar, and Navigation*, 1990, Vol. 137, pp. 102–112.
21. Ward, K.D., Baker, C.J., and Watts, S., "Maritime surveillance radar, Part I: Radar scattering from the ocean surface," *IEEE Proceedings F – Radar, Sonar, and Navigation*, 1990, Vol. 137, pp. 51–62.
22. Gini, F., Farina, A., and Montanari, M., "Vector subspace detection in compound-Gaussian clutter, Part II: Performance analysis" *IEEE Transactions on Aerospace and Electronic Systems,* 2002, Vol. 38, No. 10, pp. pp. 1312–1323.
23. Sangston, K.J. and Gerlach, K., "Coherent detection of radar targets in a non-Gaussian background," *IEEE Transactions on Aerospace and Electronic Systems,* 1994, Vol. 30, No. 2, pp. 330–340.
24. Gerlach, K., "Spatially distributed target detection in non-Gaussian clutter," *IEEE Transactions on Aerospace and Electronic Sy-*

stems, 1999, Vol. 35, No. 7, pp. 926–934.
25. Gini, F., Greco, M.V., Diani, M., and Verrazzani, L., "Performance analysis of two adaptive radar detectors against non-Gaussian real sea clutter data," *IEEE Transactions on Aerospace and Electronic Systems,* 2000, Vol. 36, No. 4, pp. 1429–1439.
26. McDonald, M. and Lycett, S., "Fast versus slow scan radar operation for coherent small target detection in sea clutter,"*IEEE Proceedings F – Radar, Sonar, and Navigation*, 2005, Vol. 152, No. 6, pp. 429–435.
27. Hu, J., Tung, W.-W., and Gao, J., "Detection of low observable targets within sea clutter by structure function based multifractal analysis," *IEEE Transactions on Antennas and Propagation,* 2006, Vol. 54, No. 1, pp.136–143.
28. Tuzlukov, V.P., "A new approach to signal detection theory," *Digital Signal Processing*, 1998, Vol. 8, No. 3, pp.166–184.
29. Tuzlukov, V.P., *Signal Processing in Noise: A New Methodology*, Minsk: IEC, 1998.
30. Tuzlukov, V.P., *Signal Detection Theory*, New York: Springer-Verlag, 2001.
31. Tuzlukov, V.P., *Signal Processing Noise*, Boca Raton, London, New York, Washington D.C.: CRC Press, Taylor & Francis Group, 2002.
32. Tuzlukov, V.P., *Signal and Image Processing in Navigational Systems*, Boca Raton, London, New York, Washington D.C.: CRC Press, Taylor & Francis Group, 2005.
33. Tuzlukov, V.P., *Signal Processing in Radar Systems*, Boca Raton, London, New York, Washington D.C. CRC Press, Taylor & Francis Group, 2012.
34. Blunt, S.D., Gerlach, K., and Heyer, J., "HRR detector for slow-moving targets in sea clutter," *IEEE Transactions on Aerospace and Electronic Systems,* 2007, Vol. 43, No. 3, pp. 965–974.